Editors' Suggestion

Equation of State and Thermometry of the 2D SU(N) Fermi-Hubbard Model

G. Pasqualetti,[1,2,3,*] O. Bettermann,[1,2,3] N. Darkwah Oppong,[1,2,3] E. Ibarra-García-Padilla,[4,5,6,7] S. Dasgupta,[4,5] R. T. Scalettar,[6] K. R. A. Hazzard,[4,5,6] I. Bloch,[1,2,3] and S. Fölling[1,2,3]

[1]*Ludwig-Maximilians-Universität, Schellingstraße 4, 80799 München, Germany*
[2]*Max-Planck-Institut für Quantenoptik, Hans-Kopfermann-Straße 1, 85748 Garching, Germany*
[3]*Munich Center for Quantum Science and Technology (MCQST), Schellingstraße 4, 80799 München, Germany*
[4]*Department of Physics and Astronomy, Rice University, Houston, Texas 77005-1892, USA*
[5]*Rice Center for Quantum Materials, Rice University, Houston, Texas 77005-1892, USA*
[6]*Department of Physics, University of California, Davis, California 95616, USA*
[7]*Department of Physics and Astronomy, San José State University, San José, California 95192, USA*

(Received 30 May 2023; accepted 9 January 2024; published 21 February 2024)

We characterize the equation of state (EoS) of the SU($N > 2$) Fermi-Hubbard Model (FHM) in a two-dimensional single-layer square optical lattice. We probe the density and the site occupation probabilities as functions of interaction strength and temperature for $N = 3$, 4, and 6. Our measurements are used as a benchmark for state-of-the-art numerical methods including determinantal quantum Monte Carlo and numerical linked cluster expansion. By probing the density fluctuations, we compare temperatures determined in a model-independent way by fitting measurements to numerically calculated EoS results, making this a particularly interesting new step in the exploration and characterization of the SU(N) FHM.

DOI: 10.1103/PhysRevLett.132.083401

The interest in the square lattice SU(2) Fermi-Hubbard Model (FHM) has been historically driven by its suitability to describing cuprate superconductors, owing to their layered character and exceptionally simple band structure near the Fermi surface. For other more complex and multiorbital materials, however, descriptions with $N > 2$ spin components have long been used, which, in addition to being of fundamental interest, provide an elegant approximation of degenerate orbitals using a higher symmetry group. Larger N systems, in particular in 2D geometries, are relevant for describing the physics of transition-metal oxides [1–3], orbitally selective Mott transitions [4–7], graphene's SU(4) spin valley symmetry [8], twisted-bilayer graphene [9–12], the Kondo effect [13,14], heavy fermion behavior [15], and achieving robust itinerant ferromagnetism [16,17]. The SU(N) FHM is a special case of the $N > 2$ models that enjoys a higher symmetry group that stabilizes quantum fluctuations [18], making it a fertile ground for theory, and constituting a baseline to more complex multiorbital models. The determination of the $N > 2$ equation of state (EoS) of the SU(N) FHM is an important milestone in the attempt of understanding its properties. However, the exponential scaling of the Hilbert space with N and the increased severity of the fermion sign problem [19] make its numerical simulation more challenging than the $N = 2$ case [20–23].

Ultracold atoms in an optical lattice have provided valuable quantum simulations of the SU(2) FHM [24]. They complement and can sometimes outperform classical simulations [25,26]. More recently, the SU($N > 2$) FHM has been successfully explored with ultracold alkaline-earthlike atoms such as ^{173}Yb or ^{87}Sr in optical lattices, which naturally feature a full SU(N) symmetry in the atomic ground state [27–35]. A substantial effort has been placed in probing the thermodynamics and the short-range correlations of the model for different spin degeneracies and lattice geometries, and experiments have gone well beyond the regime that can be calculated with theory [36–42]. However, the SU(N) generalization remains much less explored and understood compared to the SU(2) case [43]. This is particularly true in two dimensions, where the thermodynamics of the SU(2) FHM at intermediate temperatures have been studied extensively [44–60].

In this Letter, we probe the equation of state of the two-dimensional SU(N) FHM in a square lattice at intermediate temperatures in both the metallic and the Mott regime and compare our results with numerical calculations. In particular, we determine the in-lattice temperature and entropy by fitting experimental data using numerical methods such as determinantal quantum Monte Carlo (DQMC) [61,62] and numerical linked cluster expansion (NLCE) [63,64]. We additionally determine the entropies in the 2D bulk

before loading and after unloading from the lattice potential, and separately characterize the system inside the lattice with a thermometry relying on the fluctuation-dissipation theorem (FDT) based on the measurement of density fluctuations, without requiring modeling by theory.

The SU(N) FHM Hamiltonian is given by

$$\hat{H} = -t \sum_{\langle i,j \rangle,\sigma} \left(\hat{c}^{\dagger}_{i\sigma} \hat{c}_{j\sigma} + \text{H.c.} \right) + \frac{U}{2} \sum_{i,\sigma \neq \tau} \hat{n}_{i\sigma} \hat{n}_{i\tau} - \sum_{i,\sigma} \mu_i \hat{n}_{i\sigma}, \quad (1)$$

where $\hat{c}^{\dagger}_{i\sigma}$ and $\hat{c}_{i\sigma}$ represent the fermionic creation and annihilation operators at site i with spin $\sigma \in \{1 \ldots N\}$, $\hat{n}_{i\sigma} = \hat{c}^{\dagger}_{i\sigma} \hat{c}_{i\sigma}$ is the number operator, $\langle i, j \rangle$ denotes next-neighbor lattice sites, t is the hopping amplitude, U is the on-site interaction strength, and μ denotes the chemical potential, which absorbs the contribution of the trap confinement in the local density approximation [65].

In this Letter, we directly probe the local density, components of the site-occupation distribution, and the density fluctuations within the detection resolution of a few lattice sites. By differentiating the density with respect to the local chemical potential, we evaluate the isothermal compressibility $\kappa = \partial n / \partial \mu|_T$. Crucially, we implement a 2D single-layer SU(N) ensemble that we probe with perpendicular absorption imaging with a resolution of a few lattice sites. This avoids integrating over inhomogeneous stacks of 2D systems [66,67] and allows us to directly access the density profile without complex reconstruction techniques required in 3D [37] and access density fluctuations as an additional thermodynamic *in situ* observable.

In our experiment, we load a degenerate Fermi gas of ^{173}Yb with tunable $N \leq 6$ equally populated components [see Fig. 1(a)] and an entropy per particle $s/k_B \gtrsim 1.0$ into the single, horizontal layer of a vertical lattice. In this layer, we adiabatically ramp up a 2D square lattice potential with a wavelength of $\lambda = 759$ nm and a spacing of $d = \lambda/2$ [see Fig. 1(b)]. By modifying the lattice depth, we can tune the strength of the interactions. We measure the density distribution using *in situ*, saturated absorption imaging with a spatial resolution of approximately 2 μm $\approx 5d$ [68].

The measured 2D density $n(x, y)$ of an SU(6) ensemble is shown in Fig. 1(c) for different interaction strengths and the same initial state preparation in the 2D bulk (the potential without in-plane lattices). Because of the harmonic confinement generated by the Gaussian profile of the lattice beams, the chemical potential varies across the trap, sampling different regions of the EoS. For increasing interactions, and in particular when the on-site interaction is larger than the square lattice bandwidth ($U/t \gtrsim 8$), we observe the emergence of plateaus at integer density which we associate with an incompressible regime, a signature of a Mott insulating state [78].

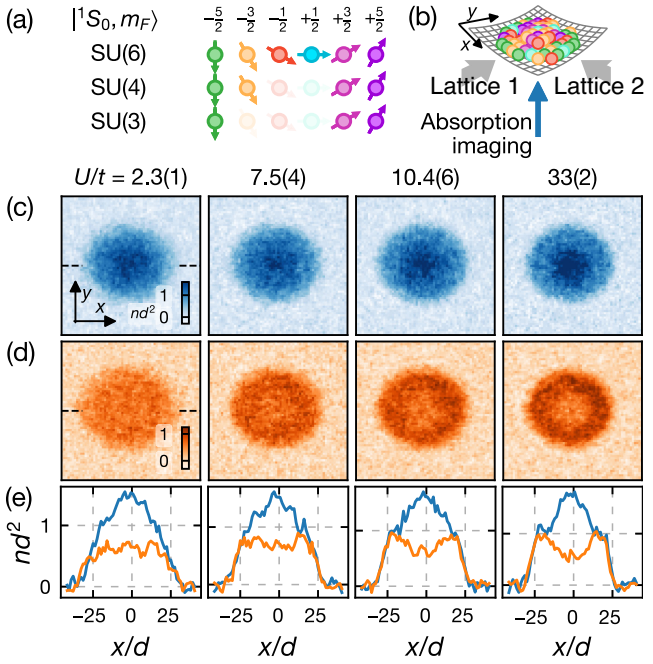

FIG. 1. Probing the 2D SU(N) Fermi-Hubbard model with ultracold atoms. (a) The $^1S_0$ ground state of ^{173}Yb naturally features an SU(6) symmetry, which can be freely tuned to $N \leq 6$ by preparing a suitable combination of the nuclear spin states $m_F = -5/2, -3/2, \ldots, +5/2$ (colored circles and arrows). (b) Schematic of the experimental setup showing a gas in a single layer 2D square lattice with harmonic confinement detected with absorption imaging along gravity. The square lattice is created by superimposing two orthogonal retro-reflected in-plane lattices. (c) Spatial distribution of the density $n(x, y)$ for $N = 6$. Each cloud shown in the horizontal frame has been prepared with the same initial entropy in the bulk and loaded into the lattice to a different U/t value. (d) Singly occupied sites after parity projection. Each horizontal frame corresponds to the same state shown in the same column of (c). (e) Density profiles for the data shown in (c) and (d) along the corresponding dashed lines in the left frames. Each image was produced using the averaging of eight shots after center of mass alignment [68].

As a distinctive probe of number squeezing effects in and close to the Mott regime [79–81], we determine the occupation number distribution by measuring the parity-projected density. After tuning U/t, we freeze the motion of the atoms by rapidly increasing the lattice depth and applying a photoassociation beam [36], which converts on-site pairs into excited-state molecules that are subsequently lost. The process removes $> 99\%$ of the on-site pairs and $\approx 5\%$ of the remaining atoms [68]. Figure 1(d) shows the distribution of the singly occupied sites corresponding to the same states of Fig. 1(c). The increase in depletion in the center with increasing interaction strength is a consequence of number squeezing to a high atom pair fraction.

To access different spin degeneracies, we prepare $N < 6$ ensembles by removing spin components using optical pumping [68]. In Figs. 2(a)–2(d), we show the EoS as a

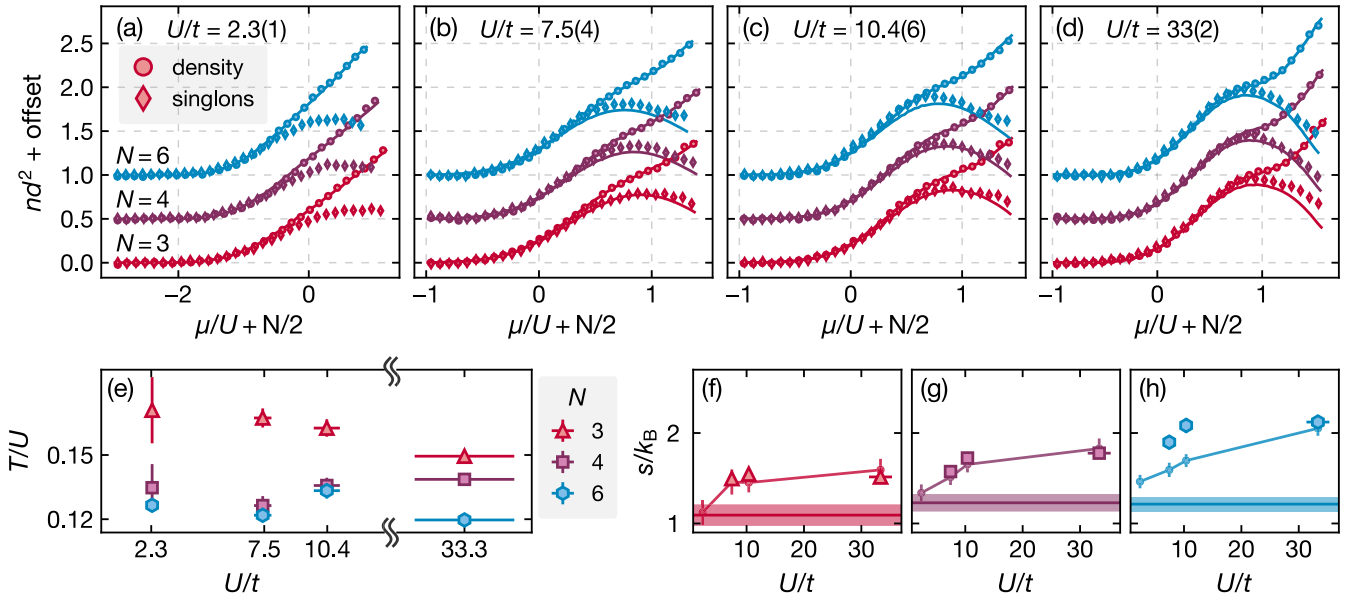

FIG. 2. Equation of state for the SU(N) Fermi-Hubbard model with $N = 6$ (blue), $N = 4$ (purple), and $N = 3$ (red). (a)–(d) Density (circles) and singly occupied sites (diamonds) as a function of the chemical potential. Data for $N = 4$ and $N = 6$ have been offset by $0.5nd^2$ and $1.0nd^2$ along the vertical axis, respectively. Continuous lines associated to the density curves correspond to the fit of the EoS calculations to the total density as described in the text. The theory used for the fit is DQMC for $U/t = 2.3(1)$ and NLCE for the other values of U/t. The results from this fit model are also used to calculate the expected pair and single-site distribution measurement. The chemical potential is defined with respect to the reference half filling [$nd^2(\mu = 0) = N/2$]. For each U/t, we fit the average of 15 frames with similar atom number after center-of-mass alignment [68]. Error bars are the standard error of the mean (s.e.m.). (e) Temperature according to the fit of the EoS shown in (a)–(d). (f)–(h) Entropy per particle. Horizontal line: entropy in the 2D bulk before loading into the lattice; triangles, squares, hexagons: entropy in the lattice according to the fit of the EoS; small circles: entropy in the 2D bulk after a round-trip experiment. The entropy in the bulk takes into account the effect of the interactions and the 3D anisotropic density of states [68]. Error bars correspond to the s.e.m. of the fit results.

function of the local chemical potential μ/U for $N \in \{6, 4, 3\}$. The chemical potential at a given location is calculated from the potential of the trap $\mu(x, y) = \mu_0 - \frac{1}{2}(\kappa_x x^2 + \kappa_y y^2)$. The exact shape of the potential is determined by fitting the density, where the trap frequencies are left as free parameters. We use a combined fit of the densities for $N = 3$, 4, and 6 for each separate U/t, but verify that separate fits for each N return values compatible with those of the combined fit. The fit of the EoS is performed in two dimensions, leaving as free parameters the temperatures $T(U/t, N)$ and the chemical potential $\mu_0(U/t, N)$ at the center of the trap. The theoretical density is convolved with the reconstructed point spread function (PSF) [68] to take into account the imaging imperfections.

For the EoS of Fig. 2, each spin mixture has been prepared with the same initial entropy per particle $s/k_B = 1.2(1)$ in the 2D bulk before ramping up the lattice. We fit and benchmark NLCE and DQMC [68] which are commonly used state-of-the-art methods for finite-temperature SU(2) Hubbard models in the regime we are considering but have only recently been extended and applied to the SU(N) experimental regime, which requires calculations away from $nd^2 = 1$ [23,41]. This is, to our knowledge, the first application of SU(N) NLCE to noninteger filling, and to the calculation of the occupancy distributions. Moreover, compared to previous works, the calculation has been extended to higher orders [68] to ensure a better convergence at low temperatures. For $U/t = 7.5(4)$ and 10.4(6) we fit both DQMC and NLCE, observing an excellent agreement between the theory and the experiment when fitting the temperature and the chemical potential at the center of the trap to the same data set with different numerical methods [68]. For $U/t = 33(2)$, we use NLCE and a high-temperature series expansion (HTSE-2), observing also in this case an excellent agreement [68]. For $U/t = 2.3(1)$, the temperature lies below the range of convergence of NLCE and we resort to DQMC alone. In Figs. 2(a)–2(d), for the cases in which we fit more than one model, we only plot the NLCE results, because the lines would overlap.

In addition to the total density, in Figs. 2(a)–2(d) we also characterize the distribution of on-site occupation numbers by removing doublons using the pair removal process described above. Experimental measurements (diamonds) are compared with the NLCE prediction (lines) based on the fit of the density, without additional free fit parameters, and agree well with the experimental data whenever available. As opposed to the $N = 2$ case, where only double occupancies are allowed, higher occupancies occur

for $N > 2$. Although the numbers of these occupancies are small for the results considered at the temperatures and chemical potentials presented here, the photoassociation technique can be used to probe triple occupancies and their dynamics [82].

The harmonic confinement of the trap returned by the density fit can be compared to the confinement obtained from an independent measurement of the oscillatory motion of the atoms in the combined dipole potentials [68]. We find a discrepancy between about 13% for $U/t = 7.5(4)$ and 40% for $U/t = 33(2)$, which is not fully explained by tolerances or the trap loading model. A possible contribution could be a lack of adiabaticity during the loading into the lattice [83–85]. However, neither varying the speed of the lattice ramps up to a factor of four (up to 1 s length) nor variations of the atom number lead to significant changes in the fit results. This would require the nonadiabatic effects to produce minimal changes in density and parity profiles [68].

In Fig. 2(e) we plot the temperatures obtained by the fits of the EoS. We observe a smaller temperature for larger N, a behavior expected due to the Pomeranchuk effect [30,86], but somewhat weaker than the ideal theoretical predictions [21,86] with the temperatures for $N = 4$ and 6 differing from each other by up to 20%. We interpret this as a consequence of the heating not depending on N during the loading process, resulting in different entropies in the lattice. This is supported by the results presented in Figs. 2(f)–2(h). We find that, despite the initial entropy in the 2D bulk before loading into the lattice being independent of N, the entropy returned by the fit of the EoS is larger for larger N, which explains the weakening of the Pomeranchuk effect. For $U/t = 2.34$ entropy results are not yet converged at those such low temperatures and therefore are not presented. We also determine the entropy per particle in the 2D bulk after a round-trip experiment, which adds an inverted ramp back to the 2D bulk system. In this case, we obtain entropies comparable to those reported by the fit in the lattice for $N = 3$ and $N = 4$ but smaller for $N = 6$, similar to previous observations [37] and potentially indicating nonadiabatic effects in the preparation or return ramp.

Complementary to the measurement of the EoS, the new possibility to directly access the density in the 2D SU(N)-system allows us to probe the density fluctuations. For an integration area of size $A \gg d^2$, the variance of the detected atom number is related to the isothermal compressibility κ and the temperature T through the fluctuation-dissipation theorem [87]:

$$\mathrm{var}\left(\int_A n\, dA\right) = k_B T \kappa A = k_B T A \left.\frac{\partial n}{\partial \mu}\right|_T . \qquad (2)$$

By measuring the density fluctuations, we can access the temperature with spatial resolution, without applying an EoS model to the dataset [60]. In Fig. 3(a) we show such density fluctuations mapped to the chemical potential for different U/t values and $N = 6$. Similar measurements for $N = 3$ and $N = 4$ are presented in the Supplemental Material [68]. For strong interactions, we observe a reduction of the fluctuations in the proximity of $nd^2 = 1$, where we expect an incompressible Mott-insulating regime. These measurements determine the temperature independently of the EoS fits, although the calibration values for the density and the trap configuration in this particular case were partially obtained from EoS-fitted datasets. Notably, the fluctuation amplitude is determined by area integration as described in Eq. (2), and therefore agrees with the thermodynamic fluctuations from the FDT as opposed to the expected on-site fluctuations $\delta\hat{n}_0^2 = \langle\hat{n}^2\rangle - \langle\hat{n}\rangle^2$ (gray dashed line). This discrepancy illustrates the role of nonvanishing short-range density correlations.

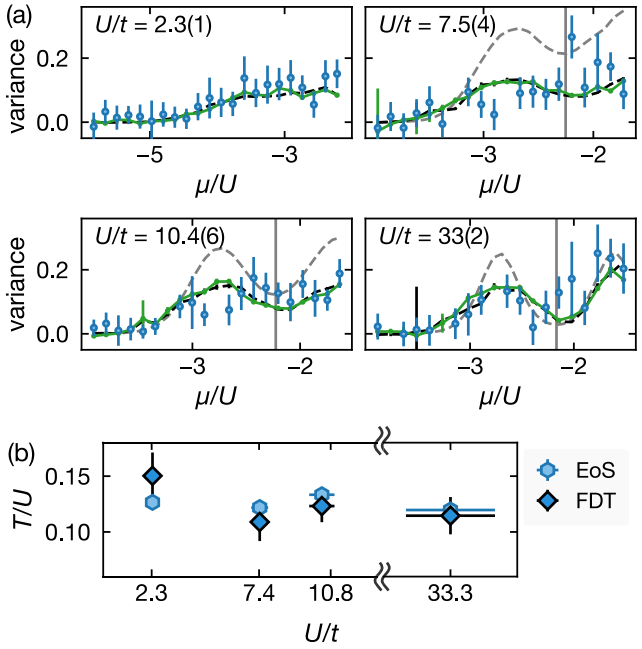

FIG. 3. (a) Measured density fluctuations (blue) for $N = 6$ as a function of the chemical potential for different interaction strengths. The data points have been obtained from the variance of 15 frames [same as Figs. 2(a)–2(d)] computed on spatially binned probe areas of size $\approx 5.1 \times 5.1 d^2$ (4×4 square camera pixels). The photon shot noise has been subtracted and a PSF correction has been taken into account [68]. The green line corresponds to the numerically differentiated compressibility κ times the temperature T_{EoS} obtained from the EoS fit of the averaged data, while the black dashed line corresponds to the theory-derived compressibility times T_{EoS}. The vertical line indicates $\mu(nd^2 = 1)$. The gray dashed line corresponds to the on-site density fluctuations $\delta n_0^2 = \langle\hat{n}^2\rangle - \langle\hat{n}\rangle^2$ calculated with NLCE for T_{EoS}. (b) Comparison of the temperatures T_{FDT} (dark blue diamonds) and T_{EoS} (light blue hexagons). Error bars are the s.e.m.

The FDT holds locally for each density. In thermal equilibrium, the ratio between the fluctuations and the compressibility is constant. We use the FDT to check this assumption and extract the temperature of the system. For this purpose, we determine the isothermal compressibility $\kappa(\mu)$ directly from the density profile data with three-point differentiation and fit the temperature T_{FDT} as the proportionality factor between the fluctuations and the compressibility. In Fig. 3(b) we compare T_{FDT} (diamonds) with the temperature T_{EoS} (hexagons) returned by the fit of the EoS. We observe a good agreement for all interactions. Moreover, we see that the residuals of the FDT analysis typically show similar temperatures at the center and at the edge of the cloud, indicating that there are no strong deviations from thermal equilibrium [68].

In conclusion, we report the measurement of the equation of state of the 2D SU(N) FHM across the Mott crossover for temperatures comparable with or below the hopping energy and we compare the experiment with state-of-the-art numerical models. Moreover, with direct access to a single 2D plane system, we can independently determine temperatures in the experiment with spatial resolution using density fluctuation analysis, which allows one to e.g. cross-check thermal equilibrium. This measurement characterizes the EoS also in regimes hard to reach by current numerical methods. When compared to the experimental data, we find the theoretical calculations describe well the properties of the SU(N) gas for the applicable range of temperatures. The temperature measurements also indicate that thermal equilibration is not inhibited even in the case of deep lattices in a temperature range where the onset of spin correlations between sites is expected.

The implementation of the directly accessible 2D ensemble, together with the accompanying theoretical description, paves the way toward more direct quantum simulation of the typically 2D models of interest in naturally occurring systems with SU($N > 2$) representations such as transition metal oxides and orbitally selective Mott transitions. An intriguing example is the case of cerium volume collapse, where there is a long-standing debate whether the single orbital Hubbard model ($N = 2$) or the double-orbital Hubbard model ($N = 4$) [88–91] is the correct description. While in the condensed matter examples the SU(N) symmetry is typically only approximately realized; cold atom representations provide an essentially exact realization of SU(N), allowing one to implement fully SU(N)-symmetric and previously purely theoretical models. It should even be possible to smoothly connect both regimes in a continuous way by controlled symmetry breaking using e.g. optical state manipulation or state-dependent potentials [32,39,92], but more generally alkaline-earthlike quantum simulations of SU(N) FHM can provide insight into the validity of the SU(N) approximation in more realistic models.

We thank Alexander Impertro for his contributions in the early phase of the experiment. We thank Hao-Tian Wei for useful conversations and the exact diagonalization code used in the NLCE. N. D. O. acknowledges funding from the International Max Planck Research School for Quantum Science and Technology. E. I. G. P. is supported by Grant No. DE-SC-0022311, funded by the U.S. Department of Energy, Office of Science, and acknowledges support from the Robert A. Welch Foundation (C-1872) and the National Science Foundation (PHY-1848304). K. H. acknowledges support from the Robert A. Welch Foundation (C-1872) and the National Science Foundation (PHY-1848304), and the W. F. Keck Foundation (Grant No. 995764). Computing resources were supported in part by the Big-Data Private-Cloud Research Cyberinfrastructure MRI award funded by NSF under Grant No. CNS-1338099 and by Rice University's Center for Research Computing (CRC). K. H.'s contribution benefited from discussions at the Aspen Center for Physics, supported by the National Science Foundation Grant No. PHY1066293, and the KITP, which was supported in part by the National Science Foundation under Grant No. NSF PHY1748958. R. T. S. is supported by Grant No. DE-SC0014671 funded by the U.S. Department of Energy, Office of Science.

*giulio.pasqualetti@lmu.de

[1] Y. Tokura and N. Nagaosa, Orbital physics in transition-metal oxides, Science **288**, 462 (2000).
[2] E. Dagotto, T. Hotta, and A. Moreo, Colossal magnetoresistant materials: The key role of phase separation, Phys. Rep. **344**, 1 (2001).
[3] Y. Q. Li, M. Ma, D. N. Shi, and F. C. Zhang, SU(4) theory for spin systems with orbital degeneracy, Phys. Rev. Lett. **81**, 3527 (1998).
[4] L. de'Medici, A. Georges, and S. Biermann, Orbital-selective Mott transition in multiband systems: Slave-spin representation and dynamical mean-field theory, Phys. Rev. B **72**, 205124 (2005).
[5] S. Florens and A. Georges, Quantum impurity solvers using a slave rotor representation, Phys. Rev. B **66**, 165111 (2002).
[6] S. Florens and A. Georges, Slave-rotor mean-field theories of strongly correlated systems and the Mott transition in finite dimensions, Phys. Rev. B **70**, 035114 (2004).
[7] P. O. Sprau, A. Kostin, A. Kreisel, A. E. Böhmer, V. Taufour, P. C. Canfield, S. Mukherjee, P. J. Hirschfeld, B. M. Andersen, and J. C. S. Davis, Discovery of orbital-selective Cooper pairing in FeSe, Science **357**, 75 (2017).
[8] M. O. Goerbig, Electronic properties of graphene in a strong magnetic field, Rev. Mod. Phys. **83**, 1193 (2011).
[9] X. Y. Xu, K. T. Law, and P. A. Lee, Kekulé valence bond order in an extended Hubbard model on the honeycomb lattice with possible applications to twisted bilayer graphene, Phys. Rev. B **98**, 121406(R) (2018).
[10] Y.-Z. You and A. Vishwanath, Superconductivity from valley fluctuations and approximate SO(4) symmetry in a

weak coupling theory of twisted bilayer graphene, npj Quantum Mater. **4**, 1 (2019).
[11] W. M. H. Natori, R. Nutakki, R. G. Pereira, and E. C. Andrade, SU(4) Heisenberg model on the honeycomb lattice with exchange-frustrated perturbations: Implications for twistronics and Mott insulators, Phys. Rev. B **100**, 205131 (2019).
[12] Y. Da Liao, J. Kang, C. N. Breiø, X. Y. Xu, H.-Q. Wu, B. M. Andersen, R. M. Fernandes, and Z. Y. Meng, Correlation-induced insulating topological phases at charge neutrality in twisted bilayer graphene, Phys. Rev. X **11**, 011014 (2021).
[13] P. Nozières and A. Blandin, Kondo effect in real metals, J. Phys. **41**, 193 (1980).
[14] D. L. Cox and A. Zawadowski, Exotic Kondo effects in metals: Magnetic ions in a crystalline electric field and tunnelling centres, Adv. Phys. **47**, 599 (1998).
[15] A. C. Hewson, *The Kondo Problem to Heavy Fermions* (Cambridge University Press, Cambridge, England, 1993).
[16] H. Katsura and A. Tanaka, Nagaoka states in the SU(N) Hubbard model, Phys. Rev. A **87**, 013617 (2013).
[17] E. Bobrow, K. Stubis, and Y. Li, Exact results on itinerant ferromagnetism and the 15-puzzle problem, Phys. Rev. B **98**, 180101(R) (2018).
[18] I. Affleck and J. B. Marston, Large-N limit of the Heisenberg-Hubbard model: Implications for high-T_c superconductors, Phys. Rev. B **37**, 3774 (1988).
[19] G. G. Batrouni and R. T. Scalettar, Anomalous decouplings and the fermion sign problem, Phys. Rev. B **42**, 2282 (1990).
[20] F. F. Assaad, Phase diagram of the half-filled two-dimensional SU(N) Hubbard-Heisenberg model: A quantum Monte Carlo study, Phys. Rev. B **71**, 075103 (2005).
[21] E. Ibarra-García-Padilla, S. Dasgupta, H.-T. Wei, S. Taie, Y. Takahashi, R. T. Scalettar, and K. R. A. Hazzard, Universal thermodynamics of an SU(N) Fermi-Hubbard model, Phys. Rev. A **104**, 043316 (2021).
[22] Seung-Sup B. Lee, J. von Delft, and A. Weichselbaum, Filling-driven Mott transition in SU(N) Hubbard models, Phys. Rev. B **97**, 165143 (2018).
[23] E. Ibarra-García-Padilla, R. Mukherjee, R. G. Hulet, K. R. A. Hazzard, T. Paiva, and R. T. Scalettar, Thermodynamics and magnetism in the two-dimensional to three-dimensional crossover of the Hubbard model, Phys. Rev. A **102**, 033340 (2020).
[24] C. Gross and I. Bloch, Quantum simulations with ultracold atoms in optical lattices, Science **357**, 995 (2017).
[25] A. Bohrdt, L. Homeier, C. Reinmoser, E. Demler, and F. Grusdt, Exploration of doped quantum magnets with ultracold atoms, Ann. Phys. (Amsterdam) **435**, 168651 (2021).
[26] A. J. Daley, I. Bloch, C. Kokail, S. Flannigan, N. Pearson, M. Troyer, and P. Zoller, Practical quantum advantage in quantum simulation, Nature (London) **607**, 667 (2022).
[27] C. Wu, J.-P. Hu, and S.-C. Zhang, Exact SO(5) symmetry in the spin-3/2 fermionic system, Phys. Rev. Lett. **91**, 186402 (2003).
[28] C. Honerkamp and W. Hofstetter, Ultracold fermions and the SU(N) Hubbard model, Phys. Rev. Lett. **92**, 170403 (2004).
[29] R. W. Cherng, G. Refael, and E. Demler, Superfluidity and magnetism in multicomponent ultracold fermions, Phys. Rev. Lett. **99**, 130406 (2007).
[30] M. A. Cazalilla, A. F. Ho, and M. Ueda, Ultracold gases of ytterbium: Ferromagnetism and Mott states in an SU(6) Fermi system, New J. Phys. **11**, 103033 (2009).
[31] M. Hermele, V. Gurarie, and A. M. Rey, Mott insulators of ultracold fermionic alkaline earth atoms: Underconstrained magnetism and chiral spin liquid, Phys. Rev. Lett. **103**, 135301 (2009).
[32] A. V. Gorshkov, M. Hermele, V. Gurarie, C. Xu, P. S. Julienne, J. Ye, P. Zoller, E. Demler, M. D. Lukin, and A. M. Rey, Two-orbital SU(N) magnetism with ultracold alkaline-earth atoms, Nat. Phys. **6**, 289 (2010).
[33] A. Sotnikov and W. Hofstetter, Magnetic ordering of three-component ultracold fermionic mixtures in optical lattices, Phys. Rev. A **89**, 063601 (2014).
[34] A. Sotnikov, Critical entropies and magnetic-phase-diagram analysis of ultracold three-component fermionic mixtures in optical lattices, Phys. Rev. A **92**, 023633 (2015).
[35] V. Unukovych and A. Sotnikov, SU(4)-symmetric Hubbard model at quarter filling: Insights from the dynamical mean-field approach, Phys. Rev. B **104**, 245106 (2021).
[36] S. Taie, R. Yamazaki, S. Sugawa, and Y. Takahashi, An SU(6) Mott insulator of an atomic Fermi gas realized by large-spin Pomeranchuk cooling, Nat. Phys. **8**, 825 (2012).
[37] C. Hofrichter, L. Riegger, F. Scazza, M. Höfer, D. R. Fernandes, I. Bloch, and S. Fölling, Direct probing of the Mott crossover in the SU(N) Fermi-Hubbard model, Phys. Rev. X **6**, 021030 (2016).
[38] H. Ozawa, S. Taie, Y. Takasu, and Y. Takahashi, Antiferromagnetic spin correlation of SU(N) Fermi gas in an optical superlattice, Phys. Rev. Lett. **121**, 225303 (2018).
[39] D. Tusi, L. Franchi, L. F. Livi, K. Baumann, D. Benedicto Orenes, L. Del Re, R. E. Barfknecht, T.-W. Zhou, M. Inguscio, G. Cappellini, M. Capone, J. Catani, and L. Fallani, Flavour-selective localization in interacting lattice fermions, Nat. Phys. **18**, 1201 (2022).
[40] B. Abeln, K. Sponselee, M. Diem, N. Pintul, K. Sengstock, and C. Becker, Interorbital interactions in an SU(2) × SU(6)-symmetric Fermi-Fermi mixture, Phys. Rev. A **103**, 033315 (2021).
[41] S. Taie, E. Ibarra-García-Padilla, N. Nishizawa, Y. Takasu, Y. Kuno, H.-T. Wei, R. T. Scalettar, K. R. A. Hazzard, and Y. Takahashi, Observation of antiferromagnetic correlations in an ultracold SU(N) Hubbard model, Nat. Phys. **18**, 1356 (2022).
[42] R. R. P. Singh and J. Oitmaa, Finite-temperature strong-coupling expansions for the SU(N) Hubbard model, Phys. Rev. A **105**, 033317 (2022).
[43] Y. Takahashi, Quantum simulation of quantum many-body systems with ultracold two-electron atoms in an optical lattice, Proc. Jpn. Acad. Ser. B **98**, 141 (2022).
[44] E. Cocchi, L. A. Miller, J. H. Drewes, M. Koschorreck, D. Pertot, F. Brennecke, and M. Köhl, Equation of state of the two-dimensional Hubbard model, Phys. Rev. Lett. **116**, 175301 (2016).
[45] J. H. Drewes, E. Cocchi, L. A. Miller, C. F. Chan, D. Pertot, F. Brennecke, and M. Köhl, Thermodynamics versus local density fluctuations in the metal-Mott-insulator crossover, Phys. Rev. Lett. **117**, 135301 (2016).
[46] J. H. Drewes, L. A. Miller, E. Cocchi, C. F. Chan, N. Wurz, M. Gall, D. Pertot, F. Brennecke, and M. Köhl,

Antiferromagnetic correlations in two-dimensional fermionic Mott-insulating and metallic phases, Phys. Rev. Lett. **118**, 170401 (2017).
[47] E. Cocchi, L. A. Miller, J. H. Drewes, C. F. Chan, D. Pertot, F. Brennecke, and M. Köhl, Measuring entropy and short-range correlations in the two-dimensional Hubbard model, Phys. Rev. X **7**, 031025 (2017).
[48] M. Boll, T. A. Hilker, G. Salomon, A. Omran, J. Nespolo, L. Pollet, I. Bloch, and C. Gross, Spin- and density-resolved microscopy of antiferromagnetic correlations in Fermi-Hubbard chains, Science **353**, 1257 (2016).
[49] T. A. Hilker, G. Salomon, F. Grusdt, A. Omran, M. Boll, E. Demler, I. Bloch, and C. Gross, Revealing hidden antiferromagnetic correlations in doped Hubbard chains via string correlators, Science **357**, 484 (2017).
[50] J. Koepsell, J. Vijayan, P. Sompet, F. Grusdt, T. A. Hilker, E. Demler, G. Salomon, I. Bloch, and C. Gross, Imaging magnetic polarons in the doped Fermi–Hubbard model, Nature (London) **572**, 358 (2019).
[51] J. Koepsell, D. Bourgund, P. Sompet, S. Hirthe, A. Bohrdt, Y. Wang, F. Grusdt, E. Demler, G. Salomon, C. Gross, and I. Bloch, Microscopic evolution of doped Mott insulators from polaronic metal to Fermi liquid, Science **374**, 82 (2021).
[52] D. Greif, M. F. Parsons, A. Mazurenko, C. S. Chiu, S. Blatt, F. Huber, G. Ji, and M. Greiner, Site-resolved imaging of a fermionic Mott insulator, Science **351**, 953 (2016).
[53] C. S. Chiu, G. Ji, A. Bohrdt, M. Xu, M. Knap, E. Demler, F. Grusdt, M. Greiner, and D. Greif, String patterns in the doped Hubbard model, Science **365**, 251 (2019).
[54] G. Ji, M. Xu, L. H. Kendrick, C. S. Chiu, J. C. Brüggenjürgen, D. Greif, A. Bohrdt, F. Grusdt, E. Demler, M. Lebrat, and M. Greiner, Coupling a mobile hole to an antiferromagnetic spin background: Transient dynamics of a magnetic polaron, Phys. Rev. X **11**, 021022 (2021).
[55] A. Mazurenko, C. S. Chiu, G. Ji, M. F. Parsons, M. Kanász-Nagy, R. Schmidt, F. Grusdt, E. Demler, D. Greif, and M. Greiner, A cold-atom Fermi-Hubbard antiferromagnet, Nature (London) **545**, 462 (2017).
[56] M. F. Parsons, A. Mazurenko, C. S. Chiu, G. Ji, D. Greif, and M. Greiner, Site-resolved measurement of the spin-correlation function in the Fermi-Hubbard model, Science **353**, 1253 (2016).
[57] L. W. Cheuk, M. A. Nichols, K. R. Lawrence, M. Okan, H. Zhang, and M. W. Zwierlein, Observation of 2D fermionic Mott insulators of ^{40}K with single-site resolution, Phys. Rev. Lett. **116**, 235301 (2016).
[58] L. W. Cheuk, M. A. Nichols, K. R. Lawrence, M. Okan, H. Zhang, E. Khatami, N. Trivedi, T. Paiva, M. Rigol, and M. W. Zwierlein, Observation of spatial charge and spin correlations in the 2D Fermi-Hubbard model, Science **353**, 1260 (2016).
[59] M. A. Nichols, L. W. Cheuk, M. Okan, T. R. Hartke, E. Mendez, T. Senthil, E. Khatami, H. Zhang, and M. W. Zwierlein, Spin transport in a Mott insulator of ultracold fermions, Science **363**, 383 (2019).
[60] T. Hartke, B. Oreg, N. Jia, and M. Zwierlein, Doublon-hole correlations and fluctuation thermometry in a Fermi-Hubbard gas, Phys. Rev. Lett. **125**, 113601 (2020).
[61] R. Blankenbecler, D. J. Scalapino, and R. L. Sugar, Monte Carlo calculations of coupled boson-fermion systems. I, Phys. Rev. D **24**, 2278 (1981).
[62] S. Sorella, S. Baroni, R. Car, and M. Parrinello, A novel technique for the simulation of interacting fermion systems, Europhys. Lett. **8**, 663 (1989).
[63] M. Rigol, T. Bryant, and R. R. P. Singh, Numerical linked-cluster approach to quantum lattice models, Phys. Rev. Lett. **97**, 187202 (2006).
[64] B. Tang, E. Khatami, and M. Rigol, A short introduction to numerical linked-cluster expansions, Comput. Phys. Commun. **184**, 557 (2013).
[65] S. Nascimbène, N. Navon, K. J. Jiang, F. Chevy, and C. Salomon, Exploring the thermodynamics of a universal Fermi gas, Nature (London) **463**, 1057 (2010).
[66] N. Darkwah Oppong, L. Riegger, O. Bettermann, M. Höfer, J. Levinsen, M. M. Parish, I. Bloch, and S. Fölling, Observation of coherent multiorbital polarons in a two-dimensional Fermi gas, Phys. Rev. Lett. **122**, 193604 (2019).
[67] N. Darkwah Oppong, G. Pasqualetti, O. Bettermann, P. Zechmann, M. Knap, I. Bloch, and S. Fölling, Probing transport and slow relaxation in the mass-imbalanced Fermi-Hubbard model, Phys. Rev. X **12**, 031026 (2022).
[68] See Supplemental Material at http://link.aps.org/supplemental/10.1103/PhysRevLett.132.083401, which includes Refs. [69–77], for additional information about the experimental methods and a detailed discussion of the numerical simulations.
[69] A. Impertro, Preparation and study of 1D and 2D many-body systems with fermionic ytterbium, Master's thesis, Ludwig-Maximilians-Universtät München, 2020.
[70] K. Hueck, N. Luick, L. Sobirey, J. Siegl, T. Lompe, and H. Moritz, Two-dimensional homogeneous Fermi gases, Phys. Rev. Lett. **120**, 060402 (2018).
[71] D. Jaksch, C. Bruder, J. I. Cirac, C. W. Gardiner, and P. Zoller, Cold bosonic atoms in optical lattices, Phys. Rev. Lett. **81**, 3108 (1998).
[72] G. Reinaudi, T. Lahaye, Z. Wang, and D. Guéry-Odelin, Strong saturation absorption imaging of dense clouds of ultracold atoms, Opt. Lett. **32**, 3143 (2007).
[73] C.-L. Hung and C. Chin, In situ imaging of atomic quantum gases, in *Quantum Gas Experiments: Exploring Many-Body States* (Imperial College Press, London, 2014), Vol. 3, Chap. 6, p. 101.
[74] J. Rui, D. Wei, A. Rubio-Abadal, S. Hollerith, J. Zeiher, D. M. Stamper-Kurn, C. Gross, and I. Bloch, A subradiant optical mirror formed by a single structured atomic layer, Nature (London) **583**, 369 (2020).
[75] J. R. Engelbrecht, M. Randeria, and L. Zhang, Landau f function for the dilute Fermi gas in two dimensions, Phys. Rev. B **45**, 10135 (1992).
[76] L. Sonderhouse, C. Sanner, R. B. Hutson, A. Goban, T. Bilitewski, L. Yan, W. R. Milner, A. M. Rey, and J. Ye, Thermodynamics of a deeply degenerate SU(N)-symmetric Fermi gas, Nat. Phys. **16**, 1216 (2020).
[77] M. Köhl, Thermometry of fermionic atoms in an optical lattice, Phys. Rev. A **73**, 031601(R) (2006).

[78] The plateau in the density profile at $1/N$ filling can be more clearly identified in the radial average of the density profile shown in Fig. S6 of the Supplemental Material.
[79] C. Orzel, A. K. Tuchman, M. L. Fenselau, M. Yasuda, and M. A. Kasevich, Squeezed states in a Bose-Einstein condensate, Science **291**, 2386 (2001).
[80] M. Greiner, O. Mandel, T. Esslinger, T. W. Hänsch, and I. Bloch, Quantum phase transition from a superfluid to a Mott insulator in a gas of ultracold atoms, Nature (London) **415**, 39 (2002).
[81] F. Gerbier, S. Fölling, A. Widera, O. Mandel, and I. Bloch, Probing number squeezing of ultracold atoms across the superfluid-Mott insulator transition, Phys. Rev. Lett. **96**, 090401 (2006).
[82] M. A. Werner, C. P. Moca, M. Kormos, Ö. Legeza, B. Dóra, and G. Zaránd, Spectroscopic evidence for engineered hadronic bound state formation in repulsive fermionic SU(N) Hubbard systems, Phys. Rev. Res. **5**, 043020 (2023).
[83] L. Bonnes, K. R. A. Hazzard, S. R. Manmana, A. M. Rey, and S. Wessel, Adiabatic loading of one-dimensional SU(N) alkaline-earth-atom fermions in optical lattices, Phys. Rev. Lett. **109**, 205305 (2012).
[84] S. S. Natu, K. R. A. Hazzard, and E. J. Mueller, Local versus global equilibration near the bosonic Mott-insulator-superfluid transition, Phys. Rev. Lett. **106**, 125301 (2011).
[85] M. Dolfi, A. Kantian, B. Bauer, and M. Troyer, Minimizing nonadiabaticities in optical-lattice loading, Phys. Rev. A **91**, 033407 (2015).
[86] K. R. A. Hazzard, V. Gurarie, M. Hermele, and A. M. Rey, High-temperature properties of fermionic alkaline-earth-metal atoms in optical lattices, Phys. Rev. A **85**, 041604(R) (2012).
[87] Q. Zhou and T.-L. Ho, Universal thermometry for quantum simulation, Phys. Rev. Lett. **106**, 225301 (2011).
[88] B. Johansson, The α-γ transition in cerium is a Mott transition, Philos. Mag. **30**, 469 (1974).
[89] J. W. Allen and R. M. Martin, Kondo volume collapse and the $\gamma \rightarrow \alpha$ transition in cerium, Phys. Rev. Lett. **49**, 1106 (1982).
[90] M. J. Lipp, Z. Jenei, H. Cynn, Y. Kono, C. Park, C. Kenney-Benson, and W. J. Evans, Anomalous elastic properties across the γ to α volume collapse in cerium, Nat. Commun. **8**, 1198 (2017).
[91] K. Held, A. K. McMahan, and R. T. Scalettar, Cerium volume collapse: Results from the merger of dynamical mean-field theory and local density approximation, Phys. Rev. Lett. **87**, 276404 (2001).
[92] W. Yi, A. J. Daley, G. Pupillo, and P. Zoller, State-dependent, addressable subwavelength lattices with cold atoms, New J. Phys. **10**, 073015 (2008).